Results in Engineering 7 (2020) 100146

Contents lists available at ScienceDirect

Results in Engineering

journal homepage: www.editorialmanager.com/rineng/Default.aspx

Turbulent heat transfer enhancement in an axially rotating pipe fitted with kenics segment mixer

Obed Y.W. Abotsi, John P. Kizito *

Department of Mechanical Engineering, North Carolina A&T State University, Greensboro, NC, 27411, USA

ARTICLE INFO

Keywords:
Rotation rate
Nusselt number
Swirl flow
Heat transfer
Kenics segment mixer

ABSTRACT

This study reports heat transfer in an axially rotating pipe fitted with Kenics segment mixer. Numerical simulations were processed with the commercial finite volume Computational Fluid Dynamics (CFD) code, ANSYS Fluent 19.2. The rotating domain was modeled with the single rotating reference frame scheme. Natural convection was considered in the numerical procedure. Computations were carried out for axial Reynolds numbers between 5000 and 25,000 at different rotation rates. Rotation rate (N) is the ratio of the rotational Reynolds number to the axial Reynolds number. Predictions revealed that the Kenics segment mixer significantly improved the heat transfer of the rotating pipe. This remarkable augmentation in heat transfer was attributed to additional swirl flow created by the inserted tape. By using the Kenics segment mixer with twist ratio of 1.75, the Nusselt number of the plain rotating pipe was augmented by 92–66% at N = 1, 74-55% at N = 3, and 60-44% at N = 5. Reduction in Nusselt number augmentation as the rotating speed of the pipe increased indicated that swirl flows induced by the Kenics segment mixer was more dominant at lower rotation rates.

1. Introduction

Rotating flows are found in several industrial systems such as flow in rotating heat exchangers, nuclear reactors, cooling channels of rotors, and turbomachines [1–3]. Many numerical and experimental investigations have been performed to examine the impact of rotation on the flow pattern and heat transfer.

Anytime flow enters a rotating pipe, tangential velocity components taking place between the moving wall and the fluid force the fluid to rotate with the pipe, resulting in a flow structure different from that found in a non-rotating pipe [4]. Pedley [5] showed that the Poiseuille flow turns out to be unstable to infinitesimal disturbances once the pipe rotates about its longitudinal axis. Pedley's results have been verified by Nagib et al. [6] with experiments and by Mackrodt [7] with numerical solutions. Cannon et al. [8] revealed that the most distinct effect of rotation was in the transitional flow region (laminar to turbulent). The average velocities and turbulence intensities in a rotating pipe was studied by Kikuyama et al. [9]. From their experiments, they showed that rotation has two contrasting effects: a destabilizing is dominant at the inlet region and a stabilizing effect that prevails as the flow proceeds downstream. Murakami et al. [10] observed the pattern of flow in an axially rotating pipe by measuring the velocity distribution across the section at different distances from the inlet. They revealed that as the rotation rate of the pipe increased, the velocity profile approached the Poiseuille flow.

Seghir-Ouali et al. [11] evaluated the influence of rotation on the convective heat transfer coefficient in an axially rotating pipe. They observed that an increase in the rotation rate of the pipe improved the convective heat transfer. Numerical studies performed by Gai et al. [12] with axial water flow revealed a rise in the pressure loss with an increment of pipe rotating speed. Chong [13] examined the heat transfer and pressure loss in the rotor-stator gap with axial airflow. His results indicated that rotation increases the heat transfer rate and pressure loss. At high rotation rates, the pressure loss due to rotation accounted for about 40% of the total system loss. Other researchers also reported a significant improvement in the heat transfer rate with rotation [14–19].

Kenics segment mixers (KSM) are widely used as passive heat transfer enhancement devices in stationary pipes/systems (N = 0) because of their steady performance, ease of installation, and low cost of operation. Heat transfer enhancement by the KSM is associated with increase in the flow velocity due to reduction of the hydraulic diameter, better thermal contact between the fluid and solid which improves the temperature gradient and generation of swirl flow for rapid fluid mixing [20]. Hobbs et al. [21,22] investigated numerically the optimization of KSM geometry

* Corresponding author.
E-mail address: jpkizito@ncat.edu (J.P. Kizito).

https://doi.org/10.1016/j.rineng.2020.100146
Received 6 May 2020; Received in revised form 17 June 2020; Accepted 20 June 2020

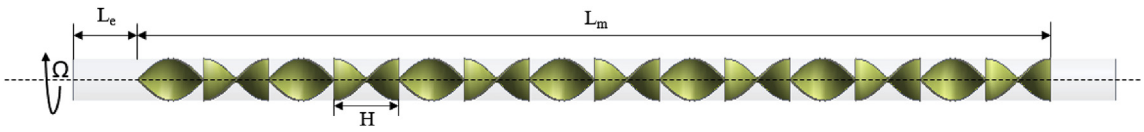

Fig. 1. Axially rotating pipe fitted with Kenics segment mixer.

using Lagrangian methods. Investigations carried out by Meng et al. [23] and Bryde et al. [24] also focused on optimizing the geometry of the KSM to augment the heat transfer. The influence of KSM on the pressure drop has been investigated by Stec et al. [25] and Kumar et al. [26]. Correlation for estimating the Nusselt number and pressure drop in stationary pipes fitted with KSM has been developed and presented [27,28]. Detailed literature review of recent developments related to KSM have been reported [29–31]. To our best knowledge, the effect of varying the twist ratio of KSM in rotating pipes has never been investigated.

The objective of the current research is to study the effect of varying the twist ratio of KSM on the heat transfer and hydraulic loss in a pipe rotating about its axis. The non-dimensionalized forms of the basic equations that describe the flow are outlined in section 2. The numerical procedure is presented in section 3 and results from simulations are discussed in section 4. Key findings are summarized in section 5.

2. Mathematical model

The flow and heat transfer processes are steady-state and are described using three conservation laws in the form of differential equations. The three-dimensional model (3D) rotates with a constant angular velocity, Ω, about its axis as depicted in Fig. 1. The incompressible Newtonian fluid is heated by imposing a uniform heat flux, q_w, on the pipe wall. The Boussinesq approximation, where the density of the fluid varies with temperature for only the buoyancy related terms in the equation was considered. The basic equations that describe the flow are presented below:

2.1. Conservation of mass

$$\frac{V_r}{r}+\frac{\partial V_r}{\partial r}+\frac{\partial V_z}{\partial z}+\frac{1}{r}\frac{\partial V_\theta}{\partial \theta}=0 \tag{1}$$

where V_r, V_θ, and V_z correspond to the velocity components in the r, θ, and z directions.

2.2. Conservation of momentum

r-component

$$\begin{aligned}&\rho\left(V_r\frac{\partial V_r}{\partial r}+\frac{V_\theta}{r}\frac{\partial V_r}{\partial \theta}-\frac{V_\theta^2}{r}+V_z\frac{\partial V_r}{\partial z}\right)\\&+\rho\left(\Omega^2 r+2\Omega V_\theta\right)\beta(T-T_\infty)\\&+\mu\left(\frac{\partial^2 V_r}{\partial r^2}+\frac{1}{r}\frac{\partial V_r}{\partial r}-\frac{V_r}{r^2}+\frac{1}{r^2}\frac{\partial^2 V_r}{\partial \theta^2}-\frac{2}{r^2}\frac{\partial V_\theta}{\partial \theta}+\frac{\partial^2 V_r}{\partial z^2}\right)\end{aligned} \tag{2}$$

θ-component

$$\begin{aligned}&\rho\left(V_r\frac{\partial V_\theta}{\partial r}+\frac{V_\theta}{r}\frac{\partial V_\theta}{\partial \theta}+\frac{V_r V_\theta}{r}+V_z\frac{\partial V_\theta}{\partial z}\right)\\&=-\frac{1}{r}\frac{\partial P}{\partial \theta}-2\rho\Omega V_r\beta(T-T_\infty)+\mu\left(\frac{\partial^2 V_\theta}{\partial r^2}+\frac{1}{r}\frac{\partial V_\theta}{\partial r}-\frac{V_\theta}{r^2}+\frac{1}{r^2}\frac{\partial^2 V_\theta}{\partial \theta^2}+\frac{2}{r^2}\frac{\partial V_r}{\partial \theta}\right.\\&\left.+\frac{\partial^2 V_\theta}{\partial z^2}\right)\end{aligned} \tag{3}$$

z-component

$$\rho\left(V_r\frac{\partial V_z}{\partial r}+\frac{V_\theta}{r}\frac{\partial V_z}{\partial \theta}+V_z\frac{\partial V_z}{\partial z}\right)=-\frac{\partial P}{\partial z}+\mu\left(\frac{\partial^2 V_z}{\partial r^2}+\frac{1}{r}\frac{\partial V_z}{\partial r}+\frac{1}{r^2}\frac{\partial^2 V_z}{\partial \theta^2}+\frac{\partial^2 V_z}{\partial z^2}\right) \tag{4}$$

where ρ is the density, μ is the dynamic viscosity, β is the coefficient of thermal expansion, P is the pressure, g is the acceleration due to gravity.

2.3. Conservation of energy

$$\rho C_p\left(V_r\frac{\partial T}{\partial r}+\frac{V_\theta}{r}\frac{\partial T}{\partial \theta}+V_z\frac{\partial T}{\partial z}\right)=k\left[\frac{\partial^2 T}{\partial r^2}+\frac{1}{r}\frac{\partial T}{\partial r}+\frac{1}{r^2}\frac{\partial^2 T}{\partial \theta^2}+\frac{\partial^2 T}{\partial z^2}\right]+\Phi \tag{5}$$

$$\begin{aligned}\Phi=&2\mu\left[\left(\frac{\partial V_r}{\partial r}\right)^2+\left(\frac{1}{r}\frac{\partial V_\theta}{\partial \theta}+\frac{V_r}{r}\right)^2+\left(\frac{\partial V_z}{\partial z}\right)^2\right]\\&+\mu\left[\left(\frac{1}{r}\frac{\partial V_r}{\partial \theta}+\frac{\partial V_\theta}{\partial r}-\frac{V_\theta}{r}\right)^2+\left(\frac{\partial V_\theta}{\partial z}+\frac{1}{r}\frac{\partial V_z}{\partial \theta}\right)^2+\left(\frac{\partial V_z}{\partial r}+\frac{\partial V_r}{\partial z}\right)^2\right]\end{aligned} \tag{6}$$

where k is the thermal conductivity, Φ is the rate of viscous dissipation, and Cp is the specific heat at constant pressure. To obtain a system of dimensionless equations, the following dimensionless variables are introduced:

$$V_r^*=\frac{V_r}{\frac{1}{2}\Omega D} \qquad V_\theta^*=\frac{V_\theta}{\frac{1}{2}\Omega D} \qquad V_z^*=\frac{V_z}{V_m}$$

$$r^*=\frac{r}{\frac{1}{2}D}, \qquad z^*=\frac{z}{L} \qquad T^*=\frac{T-T_\infty}{T_s-T_\infty}$$

$$P^*=\frac{P}{\frac{1}{4}\rho\Omega^2 D^2}$$

where L is length, and D is diameter and V_m is the axial mean velocity. The dimensionless forms of the basic flow equations are given below:

2.4. Conservation of mass (dimensionless)

$$\frac{V_r^*}{r^*}+\frac{\partial V_r^*}{\partial r^*}+\frac{1}{N(L/D)}\frac{\partial V_z^*}{\partial z^*}+\frac{1}{r^*}\frac{\partial V_\theta^*}{\partial \theta^*}=0 \tag{7}$$

2.5. Conservation of momentum (dimensionless)

r-component

$$\begin{aligned}&V_r^*\frac{\partial V_r^*}{\partial r^*}+\frac{V_\theta^*}{r^*}\frac{\partial V_r^*}{\partial \theta^*}-\frac{V_\theta^{*2}}{r^*}+\frac{1}{N(L/D)}V_z^*\frac{\partial V_r^*}{\partial z^*}=-\frac{\partial P^*}{\partial r^*}+\frac{Gr_g}{Re_\Omega^2}T^*+\left(r^*+2V_\theta^*\right)\frac{Gr_\Omega}{Re_\Omega^2}T^*\\&+\frac{4}{Re_\Omega}\left(\frac{\partial^2 V_r^*}{\partial r^{*2}}\frac{1}{r^*}\frac{\partial V_r^*}{\partial r^*}-\frac{V_r^*}{r^{*2}}+\frac{1}{r^{*2}}\frac{\partial^2 V_r^*}{\partial \theta^{*2}}-\frac{2}{r^{*2}}\frac{\partial V_\theta^*}{\partial \theta^*}+\frac{1}{4(L/D)^2}\frac{\partial^2 V_r^*}{\partial z^{*2}}\right)\end{aligned} \tag{8}$$

θ-component

$$\begin{aligned}&V_r^*\frac{\partial V_\theta^*}{\partial r^*}+\frac{V_\theta^*}{r^*}\frac{\partial V_\theta^*}{\partial \theta^*}+\frac{V_r^* V_\theta^*}{r^*}+\frac{1}{N(L/D)}V_z^*\frac{\partial V_\theta^*}{\partial z^*}=-\frac{1}{r^*}\frac{\partial P^*}{\partial \theta^*}-2V_r^*\frac{Gr_\Omega}{Re_\Omega^2}T^*\\&+\frac{4}{Re_\Omega}\left(\frac{\partial^2 V_\theta^*}{\partial r^{*2}}+\frac{1}{r^*}\frac{\partial V_\theta^*}{\partial r^*}-\frac{V_\theta^*}{r^{*2}}+\frac{1}{r^{*2}}\frac{\partial^2 V_\theta^*}{\partial \theta^{*2}}+\frac{2}{r^{*2}}\frac{\partial V_r^*}{\partial \theta^*}+\frac{1}{4(L/D)^2}\frac{\partial^2 V_\theta^*}{\partial z^{*2}}\right)\end{aligned} \tag{9}$$

z-component

$$V_r^*\frac{\partial V_z^*}{\partial r^*}+\frac{V_\theta^*}{r^*}\frac{\partial V_z^*}{\partial \theta^*}+\frac{1}{N(L/D)}\frac{\partial V_z^*}{\partial z^*}=-\frac{1}{4}\frac{N}{(L/D)}\frac{\partial P^*}{\partial z^*}+\frac{4}{Re_\Omega}\left(\frac{\partial^2 V_z^*}{\partial r^{*2}}+\frac{1}{r^*}\frac{\partial V_z^*}{\partial r^*}+\frac{1}{r^{*2}}\frac{\partial^2 V_z^*}{\partial \theta^{*2}}+\frac{1}{4(L/D)^2}\frac{\partial^2 V_z^*}{\partial z^{*2}}\right) \quad (10)$$

2.6. Conservation of energy (dimensionless)

$$V_r^*\frac{\partial T^*}{\partial r^*}+\frac{V_\theta^*}{r^*}\frac{\partial T^*}{\partial \theta^*}+\frac{1}{N(L/D)}V_z^*\frac{\partial T^*}{\partial z^*}=\frac{4}{Re_\Omega Pr}\left[\frac{\partial^2 T^*}{\partial r^{*2}}+\frac{1}{r^*}\frac{\partial T^*}{\partial r^*}+\frac{1}{r^{*2}}\frac{\partial^2 T^*}{\partial \theta^{*2}}+\frac{1}{4(L/D)^2}\frac{\partial^2 T^*}{\partial z^{*2}}\right]+\frac{Ec_\Omega}{Re_\Omega}\Phi^* \quad (11)$$

$$\Phi^*=2\left[\left(\frac{\partial V_r^*}{\partial r^*}\right)^2+\left(\frac{1}{r^*}\frac{\partial V_\theta^*}{\partial \theta^*}+\frac{V_r^*}{r^*}\right)^2+\left(\frac{1}{N(L/D)}\frac{\partial V_z^*}{\partial z^*}\right)^2\right]+\left(\frac{1}{r^*}\frac{\partial V_r^*}{\partial \theta^*}+\frac{\partial V_\theta^*}{\partial r^*}-\frac{V_\theta^*}{r^*}\right)^2+\left(\frac{1}{2(L/D)}\frac{\partial V_r^*}{\partial z^*}+\frac{2}{N}\frac{1}{r^*}\frac{\partial V_z^*}{\partial \theta^*}\right)^2+\left(\frac{2}{N}\frac{\partial V_z^*}{\partial r^*}+\frac{1}{2(L/D)}\frac{\partial V_r^*}{\partial z^*}\right)^2 \quad (12)$$

From equation (7) – (12), it is concluded that flow in an axially rotating pipe is affected by the following dimensionless parameters:

$N=\frac{Re_\Omega}{Re_a}$; rotation rate

$Re_a=\frac{V_m D}{\nu}$; axial Reynolds number

$Re_\Omega=\frac{\Omega D^2}{\nu}$; rotational Reynolds number

$Gr_g=\frac{g\beta(T_s-T_\infty)D^3}{\nu^2}$; gravitational Grashof number

$Gr_\Omega=\frac{\Omega^2\beta(T_s-T_\infty)D^4}{\nu^2}$; rotational Grashof number

$Pr=\frac{C_p\mu}{k}$; Prandtl number

$Ec_\Omega=\frac{\Omega^2 D^2}{C_p(T_s-T_\infty)}$; Eckert number

The heat transfer is characterized by the Nusselt number. The Nusselt number is calculated as:

$$Nu_x=\frac{h_x D}{k} \text{ ; local Nusselt number} \quad (13)$$

$$Nu=\frac{\int Nu_x dA_s}{\int dA_s} \text{ ; average Nusselt number} \quad (14)$$

where dA_s is the wall surface area and h_x is the convective heat transfer coefficient. The friction factor (f) describes the pressure loss across the pipe and is computed as:

$$f=\left(\frac{1}{L/D}\right)\left(\frac{2\Delta P}{\rho V_m^2}\right) \quad (15)$$

Parametric runs were formulated based on the obtained dimensionless parameters.

Table 1
Geometric parameter of the pipe with Kenics segment mixer.

Parameter	Value
Pipe length, L (mm)	800
Pipe diameter (mm)	20
Mixing zone length, L_m (mm)	700
Insert, W (mm)	20
Insert thickness, δ (mm)	1
Entrance length, L_e (mm)	50
Twist angle (^{0})	180

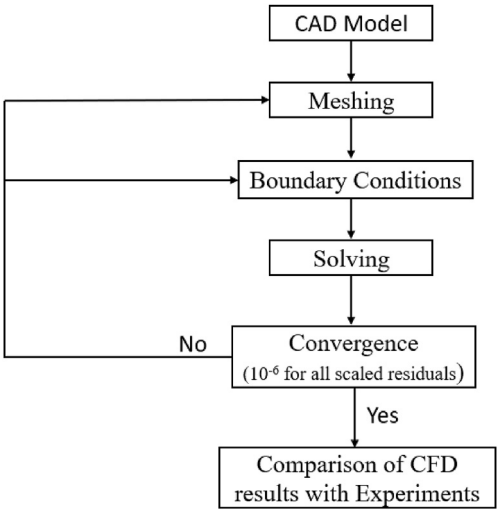

Fig. 2. Flow chart of the numerical procedure.

3. Numerical procedure

The schematic of the pipe with the Kenics segment mixer (KSM) is shown in Fig. 1. The KSM consists of alternating clockwise and anti-clockwise segments arranged axially in the pipe. Each segment is a tape that has been given 180° helical twist. The angle of intersection between the left and right twisted segments is 90°. Twist ratio (TR) is the ratio of a segment length (H) to the width (W). Three twist ratios of 1.75, 2.5, and 3.5 are investigated. The KSM is made of aluminum and has a thickness (δ) of 1 mm. Details of the geometric parameters are summarized in Table 1.

Simulations are processed using the finite volume Computational Fluid Dynamics code, ANSYS Fluent 19.2. To close the Reynolds Average Navier-Stokes (RANS) equations, the realizable k-ε turbulence model is employed. The single reference frame approach is used to model the rotating region. The coupled algorithm is used to handle the pressure-velocity coupling and the convective terms in the equations are discretized with the second-order upwind scheme. Gravity and natural conduction are included in the simulations. A convergent criterion of 10^{-6} is specified for all the scaled residuals. A flowchart of the numerical procedure is shown in Fig. 2.

A uniform heat flux of 10,000 W/m^2 is imposed on the wall of the rotating pipe. The no-slip boundary condition is specified on the wall and the surfaces of the inserted tape. The turbulence intensity at the inlet is set at 5%. The inlet temperature is set at 300 K and a pressure outlet condition of zero-gauge pressure is specified at the outlet. The axial Reynolds number which determines the inlet flow velocity is varied between 5000 and 25,000 ($5000 \leq Re_a \leq 25{,}000$) at different pipe rotation rates. Water is selected as the cooling fluid. The thermophysical properties of water are assumed to be constant and given as $\rho = 998.2$ kg/m^3, k = 0.6 W/(m-K), μ = 0.00103 kg/(m-s), and Cp = 4182 J/(kg-K) respectively. The enhanced wall function is adopted for near-wall treatment. For each configuration, the y + value < 1.

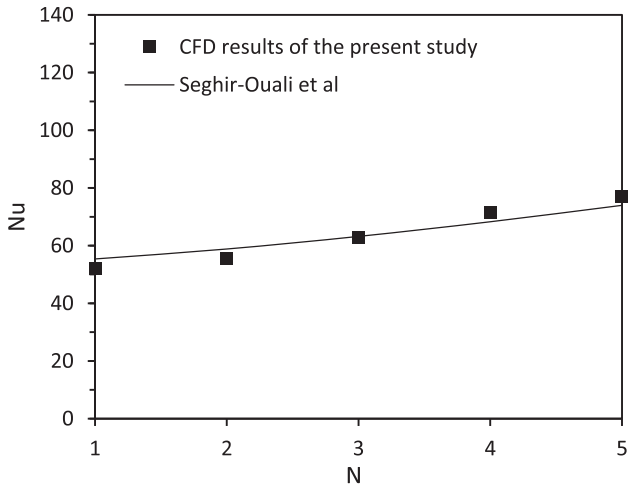

Fig. 3. Verification of Nusselt number of the plain rotating pipe ($Re_a = 5000$).

A grid sensitivity analysis was carried out to confirm that the numerical solution is independent of the grid size. Five different grid numbers: 157,984, 237,964, 391,685, 493,057, and 641,586 for the pipe with KSM (TR = 1.75) are evaluated at N = 1 and $Re_a = 5000$. The variation in the average Nusselt number and friction factor among the grid numbers 391685 and 641,586 is less than 1%. Considering the computational cost, the grid with 391,685 elements was chosen for the study.

To validate the reliability of the numerical model, simulation results are compared with the well-known empirical correlation for flow in an axially rotating pipe. Seghir-Ouali et al.'s correlation of the Nusselt number in an axially rotating pipe is shown below [11]:

$$Nu = 0.01963Re_a^{0.9285} + 8.5101x10^{-6}Re_{\Omega}^{1.4513}$$

$$0 < Re_a < 3 \times 10^4 \text{ and } 1.6 < Re_{\Omega} < 2.77 \times 10^5$$

The comparison between the numerical results of this current study and the standard correlation is presented in Fig. 3. The deviation of the predictions for the Nusselt number is within ±6%. This great agreement between the simulation results and the empirical correlation implies that the present numerical model has reasonable accuracy.

4. Results and discussion

The predicted flow structure of the velocity and temperature fields of the pipe with KSM are shown in Fig. 4 and Fig. 5 for rotation rate of (N = 1) and axial Reynolds number of 5000. In the plain rotating pipe, higher speed flows appear in the core region while lower speed flows occur near the pipe wall which results in a thick thermal boundary layer. The inserted tape induces swirl and partitions the flow. Reducing the twist ratio (TR) of the KSM intensified the swirl flow. Swirl improves flow turbulence and promotes thermal boundary layer disruption [32–36]. The KSM insert with TR of 1.75 produced the strongest swirl and thus has the largest flow velocity as shown in Fig. 4. Consequently, heat dissipates faster in the KSM with TR of 1.75.

The variation of the Nusselt number against the axial Reynolds number is illustrated in Fig. 6 (a) for the KSM at different twist ratios (TR). Generally, increasing the rotation rate of the pipe increases the Nusselt number. Rotation introduces Coriolis and centrifugal acceleration components which creates a density gradient. This causes relatively warmer fluid at the pipe wall to move inwards and for cooler fluid at the center to move outwards.

Interactions between the Coriolis and centrifugal forces and the density gradient yield a complex secondary flow. The intensity of secondary flow increases with the increase of the rotation rate. It was also noticed that the increase of the axial Reynolds number enhanced the Nusselt number. This improvement was due to the rise of the turbulent intensities from the increase of the axial Reynolds number which resulted in augmentation of the convective heat transfer.

It was evident from Fig. 6 (a) that the KSM significantly improved the heat transfer of the rotating pipe. This remarkable augmentation in the Nusselt number was linked to the right- and left-hand arrangement of elements in the KSM which improved mixing near the edges of the tape

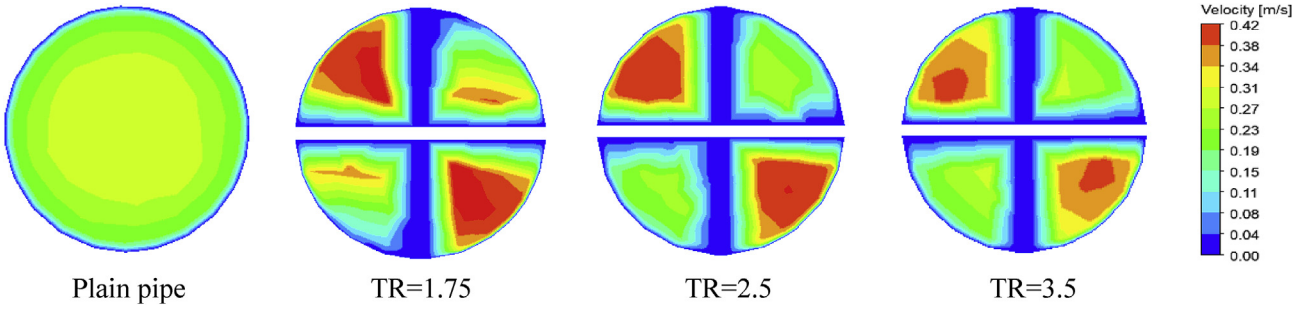

Fig. 4. Contour plots of velocity field of the pipe with/without KSM at z/L = 0.5 (N = 1; $Re_a = 5000$).

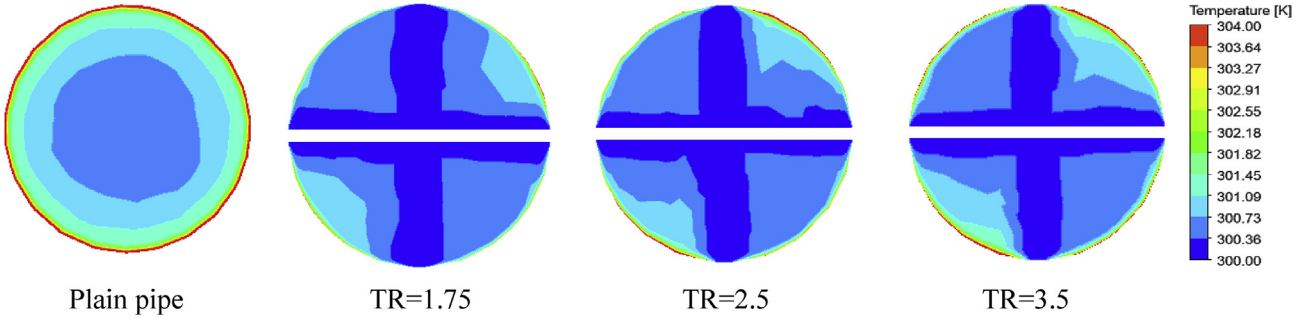

Fig. 5. Contour plot of temperature gradient of the pipe with/without KSM at z/L = 0.5 (N = 1; $Re_a = 5000$).

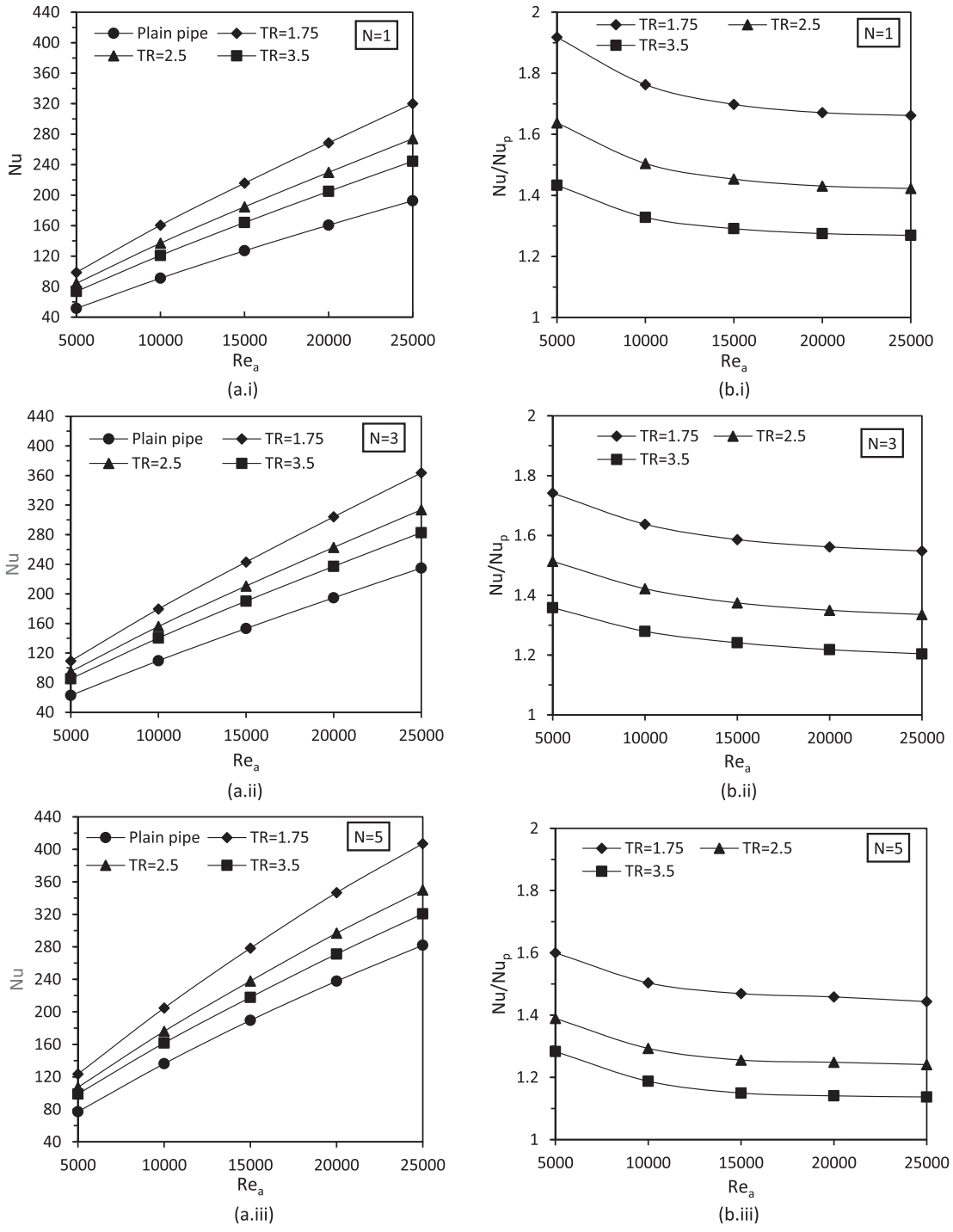

Fig. 6. The effect of Kenics segment mixer on the (a) Nusselt number (Nu) and (b) Nusselt number ratio (Nu/Nu_p) at different rotation rates.

and created additional swirl flow. Simulation results revealed enhancement in the heat transfer rate as the twist ratio of the inserted tape decreased. This can be explained by the fact that smaller TR produces stronger swirl flows, leading to a better convective heat transfer. The flow residence time also rises with an increase in the intensity of the swirl flow [37,38]. For the range of axial Reynolds number studied, the KSM with TR of 1.75 enhanced the Nusselt number of the plain pipe by approximately 92–66% at N = 1, 74-55% at N = 3 and 60-44% at N = 5. The effectiveness of the improvement in heat transfer in the pipe equipped with KSM relative to the plain pipe (Nu/Nu_p) is presented in Fig. 6 (b). The Nusselt number ratio for all cases studied was higher than 1 which represents a valuable gain in the heat transfer. The results showed a reduction in heat transfer enhancement with increasing rotation rate. This implied that the extra swirl flow that was generated by the insert was more relevant at lower rotation rates.

Fig. 7 depicts the variations of the friction factor versus the axial Reynolds number for the pipe with KSM of different twist ratios (TR). From Fig. 7, it was noted that the friction factor increases with the increase of the rotation rate. This increment was linked to the introduction of swirling velocity components from the rotating pipe wall which created large pressure gradients along the radial direction. The calculated friction factor of the pipe with KSM was higher than those obtained in the plain pipe. This was because of flow blockage, larger contact surface area, and an increase in the turbulence kinetic energy. According to Fig. 7,

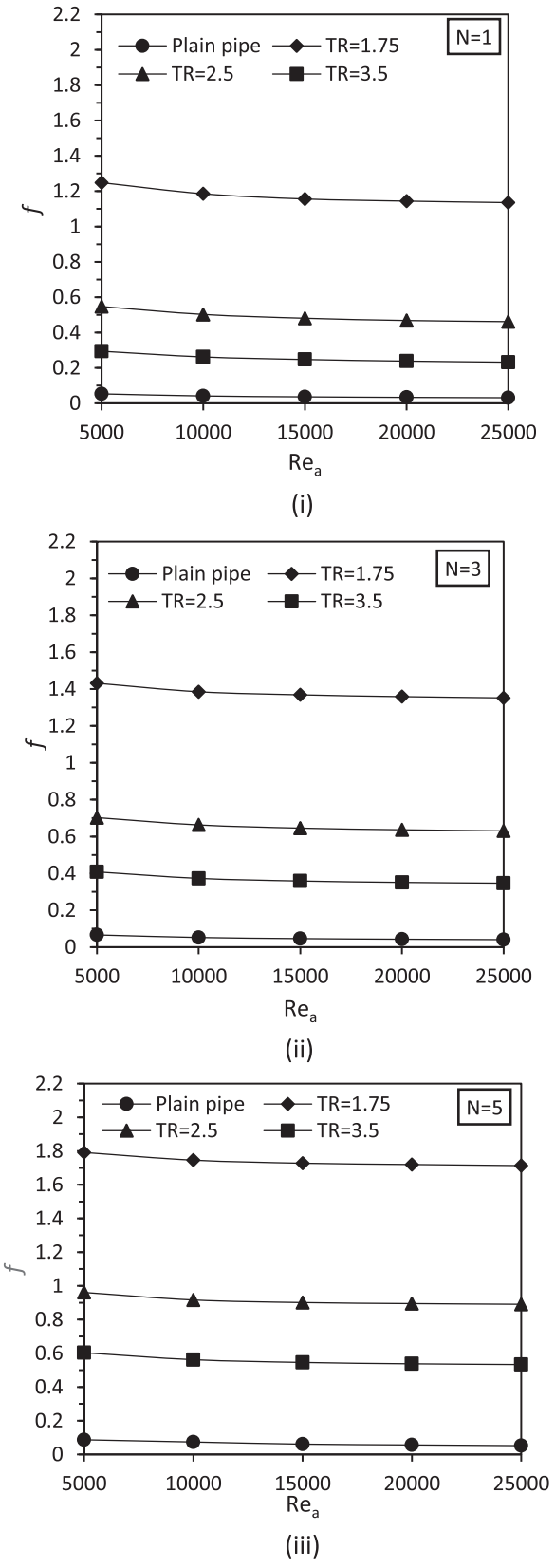

Fig. 7. The effect of Kenics segment mixer on the friction factor at different rotation rate.

decreasing the TR of the insert increased the friction factor. The friction factor of the pipe with KSM at TR = 1.75, TR = 2.5, and TR = 3.5 was increased by 20, 11, and 7 times, respectively, in comparison to the plain pipe at rotation rate of 5 (N = 5). This was because smaller twist ratios created stronger swirl flow which resulted in higher viscous losses near the pipe wall.

5. Conclusion

Turbulent heat transfer in an axially rotating pipe fitted with Kenics segment mixer has been studied numerically. The impact of parameters such as rotation rate and twist ratio have also been examined. The results showed that the Kenics segment mixer enhanced the heat transfer rate of the plain pipe significantly with a corresponding increase in the friction factor. Improvement in the heat transfer rate was attributed to extra swirl flow created by the Kenics segment mixer. It was found that as the twist ratio of the insert decreased, the strength of the swirl flow increased. The Kenics segment mixer with twist ratio of 1.75 augmented the Nusselt number of the plain pipe by 92–66% at rotation rate of 1, 74-55% at rotation rate of 3 and 60-44% at rotation rate of 5. Reduction in heat transfer enhancement as the rotation rate of the pipe increased indicated that swirl flows created by the Kenics segment mixer was more dominant at lower rotation rates.

Author contribution

Obed Y.W. Abotsi: Conceptualization, Investigation, Methodology, Validation, Writing - original draft. John P. Kizito: Supervision, Funding acquisition, Resources, Project administration

Declaration of competing interest

Authors have no conflict of interest.

Acknowledgment

We acknowledge the support from NASA NNH16ZEA001 N: Electric Propulsion: Challenges and Opportunities.

Nomenclature

A_s	Infinitesimal area of the wall (m^2)
C_p	specific heat at constant pressure (J/kg-K)
f	friction factor
D	diameter of the pipe (m)
g	gravity (m/s^2)
Gr_g	gravitational Grashof number
Gr_Ω	rotational Grashof number
h	convective heat transfer coefficient (W/m^2-K)
L	Length of the pipe (m)
L_e	entrance length (m)
L_m	mixing zone length (m)
N	rotation rate
Nu	average Nusselt number
P	Pressure (Pa)
Pr	Prandtl number
q_w	wall heat flux (W/m^2)
Re_a	axial Reynolds number
Re_Ω	rotational Reynolds number
H	length of a single mixing segment/pitch (m)
W	width of inserted tape (m)
k	thermal conductivity (W/m-K)
T	Temperature (K)
V_r, V_θ and V_z	velocity components in the r, θ and z direction (m/s)
V_m	mean axial flow velocity (m/s)

Greek symbols

δ	thickness of the inserted tape (m)
ρ	density (kg/m3)
μ	dynamic viscosity (kg/m-s)
β	coefficient of thermal expansion (K^{-1})
Ω	angular velocity(s^{-1})
ν	kinematic viscosity (m^2/s)

References

[1] W. Yang, S. Fann, J.H. Kim, Heat and fluid flow inside rotating channels, ASME. Appl. Mech. Rev. 47 (8) (1994) 367–396.

[2] M. Ould-Rouiss, A. Dries, A. Mazouz, Numerical predictions of turbulent heat transfer for air flow in rotating pipe, Int. J. Heat Fluid Flow 31 (4) (2010) 507–517.

[3] S. Hirai, T. Takagi, M. Matsumoto, Predictions of the laminarization phenomena in an axially rotating pipe flow, ASME. J. Fluids Eng. 110 (4) (1988) 424–430.

[4] G. Reich, H. Beer, Fluid flow and heat transfer in an axially rotating pipe: effect of rotation on turbulent pipe flow, Int. J. Heat Mass Tran. 32 (3) (1989) 551–562.

[5] T.J. Pedley, On the instability of viscous flow in a rapidly rotating pipe, J. Fluid Mech. 35 (1) (1969) 97–115.

[6] H.M. Nagib, Z. Lavan, A.A. Fejer, L. Wolf Jr., Stability of pipe flow with superposed solid body rotation, Phys. Fluid. 14 (4) (1971) 766–768.

[7] P.A. Mackrodt, Stability of Hagen-Poiseuille flow with superimposed rigid rotation, J. Fluid Mech. 73 (1) (1976) 153–164.

[8] J.N. Cannon, W.M. Kays, Heat transfer to a fluid flowing inside a pipe rotating about its longitudinal Axis, ASME. J. Heat Transfer 91 (1) (1969) 135–139.

[9] K. Kikuyama, M. Murakami, K. Nishibori, Development of three-dimensional turbulent boundary layer in an axially rotating pipe, ASME. J. Fluids Eng. 105 (2) (1983) 154–160.

[10] M. Murakami, K. Kikuyama, Turbulent flow in axially rotating pipes, ASME. J. Fluids Eng. 102 (1) (1980) 97–103.

[11] S. Seghir-Ouali, D. Saury, S. Harmand, O. Phillipart, D. Laloy, Convective heat transfer inside a rotating cylinder with an axial air flow, Int. J. Therm. Sci. 45 (12) (2006) 1166–1178.

[12] Y. Gai, M. Kimiabeigi, Y.C. Chong, J. Goss, M.C. Kulan, J.D. Widmer, A. Steven, D.A. Staton, Pressure loss modelling in a water-cooled hollow-shaft rotor for an automotive traction motor, in: IEEE: Proceedings of the Thirteenth International Conference on Electrical Machines, Alexandroupoli, 2018, pp. 1297–1302.

[13] Y.C. Chong, Thermal Analysis and Air Flow Modeling of Electrical Machines, PhD Thesis, University of Edinburgh, Edinburgh, 2015.

[14] J.F. Humphreys, W.D. Morris, H. Barrow, Convection heat transfer in the entry region of a tube which revolves about an axis parallel to itself, Int. J. Heat Mass Tran. 10 (3) (1967) 333–340.

[15] O.Y. Abotsi, J.P. Kizito, Heat transfer enhancement in an axially rotating pipe with twisted tape insert, Am. J. Mech. Eng. 8 (2020) 1–8.

[16] N. Wataru, Forced convective heat transfer in a straight pipe rotating around a parallel axis, Int. J. Heat Mass Tran. 11 (7) (1968) 1185–1201.

[17] F. Song, D. Ewing, C.Y. Ching, Experimental investigation on the heat transfer characteristics of axial rotating heat pipes, Int. J. Heat Mass Tran. 47 (22) (2014) 4721–4731.

[18] M. Hettegger, B. Streibl, O. Biro, H. Neudorfer, Measurements and simulations of the convective heat transfer coefficients on the end windings of an electrical machine, IEEE Trans. Ind. Electron. 59 (5) (2011) 2299–2308.

[19] P. Hanafizadeh, S. Karbalaee, R. Attarpour, M. Ashjaee, A criterion for the effect of parallel mode rotation on non-isothermal flow through square channel, Int. J. Heat Mass Tran. 139 (2019) 343–350.

[20] H. Meng, G. Zhu, Y. Yu, Z. Wang, J. Wu, The effect of symmetrical perforated holes on the turbulent heat transfer in the static mixer with modified Kenics segments, Int. J. Heat Mass Tran. 99 (2016) 647–659.

[21] D.M. Hobbs, F.J. Muzzio, Reynolds number effects on laminar mixing in the Kenics static mixer, Chem. Eng. J. 70 (2) (1998) 93–104.

[22] D.M. Hobbs, F.J. Muzzio, Effects of injection location, flow ratio and geometry on Kenics mixer performance, AIChE J. 43 (12) (1997) 3121–3132.

[23] H. Meng, M. Song, Y. Yu, F. Wang, J. Wu, Chaotic mixing characteristics in static mixers with different axial twisted-tape inserts, Can. J. Chem. Eng. 93 (10) (2015) 1849–1859.

[24] O. Byrde, M.L. Sawley, Optimization of a Kenics static mixer for non-creeping flow conditions, Chem. Eng. J. 72 (2) (1999) 163–169.

[25] M. Stec, P.M. Synowiec, Study of fluid dynamic conditions in the selected static mixers part I-research of pressure drop, Can. J. Chem. Eng. 95 (11) (2017) 2156–2167.

[26] V. Kumar, V. Shirke, K.D.P. Nigam, Performance of Kenics static mixer over a wide range of Reynolds number, Chem. Eng. J. 139 (2) (2008) 284–295.

[27] H.S. Song, S.P. Han, A general correlation for pressure drop in a Kenics static mixer, Chem. Eng. Sci. 60 (21) (2005) 5696–5704.

[28] P. Joshi, K.D.P. Nigam, E.B. Nauman, The Kenics static mixer: new data and proposed correlations, Chem. Eng. J. Biochem. Eng. J. 59 (3) (1995) 265–271.

[29] A. Ghanem, T. Lemenand, D. Della Valle, H. Peerhossaini, Static mixers: mechanisms, applications, and characterization methods–A review, Chem. Eng. Res. Des. 92 (2) (2014) 205–228.

[30] H.E. Meijer, M.K. Singh, P.D. Anderson, On the performance of static mixers: a quantitative comparison, Prog. Polym. Sci. 37 (10) (2012) 1333–1349.

[31] R.K. Thakur, C. Vial, K.D.P. Nigam, E.B. Nauman, G. Djelveh, Static mixers in the process industries—a review, Chem. Eng. Res. Des. 81 (7) (2003) 787–826.

[32] J.D. Moya-Rico, A.E. Molina, J.F. Belmonte, J.C. Tendero, J.A. Almendros-Ibáñez, Experimental characterization of a double tube heat exchanger with inserted twisted tape elements, Appl. Therm. Eng. (2020) 115234.

[33] M. Rahimi, S.R. Shabanian, A.A. Alsairafi, Experimental and CFD studies on heat transfer and friction factor characteristics of a tube equipped with modified twisted tape inserts, Chem. Eng. Process: Process Intensification 48 (3) (2009) 762–770.

[34] H. Meng, M. Han, Y. Yu, Z. Wang, J. Wu, Numerical evaluations on the characteristics of turbulent flow and heat transfer in the Lightnin static mixer, Int. J. Heat Mass Tran. 156 (2020) 119788.

[35] S.K. Saha, A. Dutta, S.K. Dhal, Friction and heat transfer characteristics of laminar swirl flow through a circular tube fitted with regularly spaced twisted-tape elements, Int. J. Heat Mass Tran. 44 (22) (2001) 4211–4223.

[36] P. Sivashanmugam, S. Suresh, Experimental studies on heat transfer and friction factor characteristics of turbulent flow through a circular tube fitted with regularly spaced helical screw-tape inserts, Appl. Therm. Eng. 27 (8-9) (2007) 1311–1319.

[37] S. Eiamsa-ard, C. Thianpong, P. Promvonge, Experimental investigation of heat transfer and flow friction in a circular tube fitted with regularly spaced twisted tape elements, Int. Commun. Heat Mass Tran. 33 (10) (2006) 1225–1233.

[38] S. Eiamsa-Ard, C. Thianpong, P. Eiamsa-Ard, Turbulent heat transfer enhancement by counter/co-swirling flow in a tube fitted with twin twisted tapes, Exp. Therm. Fluid Sci. 34 (1) (2010) 53–62.